FUDMA Journal of Sciences (FJS)
ISSN online: 2616-1370
ISSN print: 2645 - 2944
Vol. 8 No. 5, October, 2024, pp 193 - 200
DOI: https://doi.org/10.33003/fjs-2024-0805-2652

ANALYTICAL STUDY ON FULLY DEVELOPED MIXED CONVECTION COUETTE FLOW IN A VERTICAL CHANNEL WITH VISCOUS DISSIPATION EFFECT

***[1]Tafida M. Kabir, [2]Ayuba M. Umar and [1]Usman M. Iyabo**

[1]Department of Mathematics Federal University of Education, Zaria, Nigeria
[2]Division of Agricultural Colleges Ahmadu Bello University, Zaria, Nigeria

*Corresponding authors' email: mktafida.555@gmail.com

ABSTRACT
The study of mixed convection flow in a vertical channel with viscous dissipation has been examined. To solve the governing energy and momentum equations, the Homotopy perturbation method was employed. Graphs were generated to analyze the impact of the governing flow parameters. Numerical values for skin friction, rate of heat transfer, and mass flux were estimated. The study revealed that an increase in mixed convection expands the reverse flow region and raises the critical value of mixed convection that leads to flow reversal. Additionally, both fluid temperature and velocity rise with increased viscous dissipation, as higher viscous dissipative heat elevates temperature, subsequently increasing the buoyancy force.

Keywords: Couette flow, Mixed convection, Viscous dissipation, Homotopy perturbation method, Vertical channel

INTRODUCTION

The study of mixed convection flow is a fundamental issue in fluid dynamics, attracting significant interest due to its diverse applications. These range from cooling systems in nuclear reactors and the dispersion of chemical pollutants to environmental concerns, oceanography, geophysics, and lubrication industries. Research on natural convection flow and viscous dissipation in various media is crucial. Viscous dissipation refers to the internal mechanical energy generated by the continuous interaction of fluid particles, which is irreversibly transformed into kinetic energy. Gebhart (1962) was the first to highlight the impact of viscous dissipation on natural convection flow, concluding that the energy generated internally cannot be overlooked in scenarios involving strong gravitational forces or fluids with a high Prandtl number.

Ajibade and Princely (2020) examined the effects of viscous dissipation on steady natural convection in a vertical channel, demonstrating that an increase in viscous dissipation leads to higher fluid velocity and temperature within the channel. Kairi et al. (2011) investigated the influence of viscous dissipation on a Non-Newtonian fluid and found that it significantly affects temperature, velocity, and heat transfer coefficients. Yusuf and Ajibade (2020) explored the combined effects of variable viscosity, viscous dissipation, and thermal radiation on unsteady natural convection Couette flow through a vertical porous channel, reporting that both fluid temperature and velocity rise with increasing viscous dissipation. Ajibade and Tafida (2022) focused on the impact of viscous dissipation in steady natural convection Couette flow with a convective boundary condition, concluding that fluid temperature increases with greater viscous dissipation, while fluid velocity shows the opposite trend. Fahad et al. (2017) studied the combined effects of viscous dissipation and radiation on unsteady natural convection fluid, finding that the velocity and temperature distributions remain similar as viscous dissipation increases.

Ajibade and Tafida (2020) examined how variations in viscosity and thermal conductivity affect steady mixed convection Couette flow and heat transfer, concluding that a higher mixed convection parameter can induce reverse flow. Tafida and Ajibade (2020) studied the impacts of variable viscosity and viscous dissipation on free convective Couette flow in a vertical channel using the Homotopy perturbation method, reporting that viscous dissipation increases both fluid velocity and temperature. Muawiya and Tafida (2019) looked into the effects of viscous dissipation on steady natural convection Couette flow, finding that mass flux rises with increased viscous dissipation. Ajibade et al. (2021) conducted an analytical study on the effects of viscous dissipation in steady natural convection Couette flow, concluding that the velocity profile decreases near the cold plate as viscous dissipation increases. Nur et al. (2022) investigated magnetohydrodynamic mixed convection flow of a hybrid nanofluid over a permeable vertical flat plate, noting that opposing flow due to the mixed convection parameter can enhance heat transfer. Henniche and Abdelkader (2020) studied mixed convection in a vertical channel with staggered inclined baffles, concluding that heat transfer rates and skin friction increase with higher Reynolds numbers and lower Grashof numbers. Muneer et al. (2020) explored the effect of driven sidewalls on mixed convection in an open trapezoidal cavity with a channel.

Essam and Mohammed (2021) examined mixed convection of a hybrid nanofluid in a vertical channel influenced by thermal radiative flux, demonstrating that the rate of heat transfer varies with changes in relevant parameters. Sheid et al. (2023) investigated convective heat transfer using Casson nanofluid over a vertical plate, reporting that the thickness of the velocity boundary layer decreases as the Prandtl number increases. Abdulhakeem et al. (2022) found that both the ferrohydrodynamic interaction parameter and the rotational parameter enhance temperature and concentration levels. Yusuf and Ajibade (2018) concluded that fluid velocity and temperature rise with increasing thermal radiation.

The homotopy perturbation method was introduced by He (1999) as a technique for solving linear, nonlinear, and coupled ordinary and partial differential equations. Biazar and Ghazvini (2008) applied the method to hyperbolic partial differential equations, demonstrating its high accuracy and potential effectiveness. Hamida et al. (2023) explored the use of the homotopy perturbation method to model the spread of COVID-19, asserting its suitability for solving systems of nonlinear differential equations. Shijun (2005) compared the homotopy analysis method with the homotopy perturbation method, highlighting that while the latter requires a sufficiently good initial guess, this is not essential for the

former. Tapas and Dilip (2023) developed an optimal and modified version of the homotopy perturbation method for strongly nonlinear differential equations, noting that its effectiveness is highly reliant on the transformation applied. Gouder et al. (2022) utilized the homotopy perturbation method to solve a wave equation, concluding that it yields accurate solutions and converges faster with less computational effort.

MATERIALS AND METHODS

We consider a steady flow of an incompressible fluid with viscous dissipation between two vertical parallel plates positioned at $y^* = 0$ and $y^* = h$ with the uniform temperature of θ_1 and θ_0 on the hot and cold walls is considered. The flow is assumed to be in the $x^* -$ direction which is taken vertically upward along the vertical plates and $y^* -$ axis is taken normal to the plates as shown in figure 1. The plates have infinite lengths and as result, the velocity and temperature fields are only the function of y^*

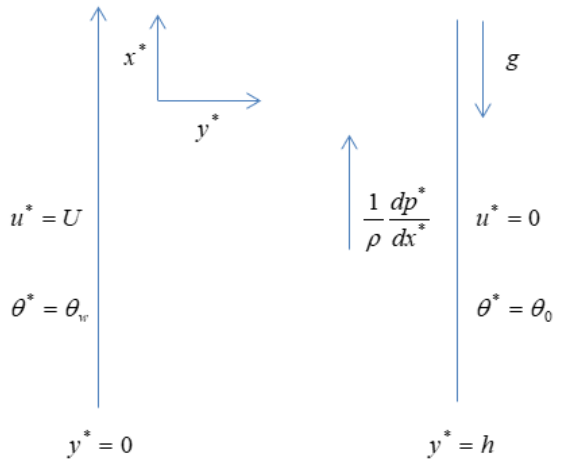

Figure 1: Schematic diagram of the problem

The mathematical model that captures the flow formation and heat transfer in a vertical channel under the Boussinesq's approximation is governed by the following equations:

$$\alpha\frac{d^2\theta^*}{dy^{*2}}+\frac{\mu^*}{\rho cp}\left(\frac{du^*}{dy^*}\right)^2=0, \quad (1)$$

$$\nu\frac{d^2u^*}{dy^{*2}}+g\beta(\theta^*-\theta_0)-\frac{1}{\rho}\frac{dP^*}{dx^*}=0. \quad (2)$$

The boundary conditions for these equations are:

$$u^*=U,\ \ \theta^*=\theta_w \text{ at } y^*=0$$
$$u^*=0 \qquad \theta^*=\theta_0 \text{ at } y^*=h. \quad (3)$$

Given that the quantities involved have different dimensions, we introduce certain dimensionless variables to transform the governing equations and boundary conditions into a dimensionless form. The dimensionless quantities used in equations (1) – (2) and the boundary condition (3) are:

$$y=\frac{y^*}{h}, u=\frac{u^*}{U}, \theta=\frac{\theta^*-\theta_0}{\theta_w-\theta_0}, Gr=\frac{g\beta h^3(\theta_w-\theta_0)}{\nu^2}, Ec=\frac{U^2}{c_p(\theta_w-\theta_0)},$$

$$Pr=\frac{\mu cp}{k}, x=\frac{x^*\nu}{Uh^2},\ P=\frac{P^*}{\rho U^2}\ \ ,Re=\frac{Uh}{\nu} \quad (4)$$

Here, y represents the dimensionless coordinate normal to the channel walls, u is the dimensionless velocity, θ is the dimensionless temperature, $Gre=\frac{Gr}{Re}$ is the ratio of the Grashof number to Reynolds number, and Ec represents the viscous dissipation. Using these definitions, equations (1) to (3) can be rewritten in the following non-dimensional forms:

$$\frac{d^2\theta}{dy^2}+Ec\,Pr\left(\frac{du}{dy}\right)^2=0, \quad (5)$$

$$\frac{d^2u}{dy^2}+Gre\theta-\frac{dp}{dx}=0, \quad (6)$$

The non-dimensional forms of the boundary conditions are:

$$u=1, \theta=1, \text{at } y=0$$
$$u=0, \theta=0, \text{at } y=1. \quad (7)$$

Method of Solution

To solve the problem using the Homotopy Perturbation Method, we construct a convex homotopy for the energy and momentum equations. Consequently, in the absence of an initial approximation, the equation takes the following form:

$$\frac{d^2\theta}{dy^2}=p\left[-Ec\,Pr\left(\frac{du}{dy}\right)^2\right] \quad (8)$$

such that

$$\theta=\theta_0+p\theta_1+p^2\theta_2+p^3\theta_3+\ldots \quad (9)$$

Substituting equation (9) into equation (8), we obtain

$$\frac{d^2\theta_0}{dy^2}+p\frac{d^2\theta_1}{dy^2}+p^2\frac{d^2\theta_2}{dy^2}+\ldots=-p\left(Ec\,Pr\left(\frac{du_0}{dy}\right)^2\right)$$
$$-p^2\left(2Ec\,Pr\left(\frac{du_0}{dy}.\frac{du_1}{dy}\right)\right) \quad (10)$$
$$-p^3\left(2Ec\,Pr\left(\frac{du_0}{dy}.\frac{du_2}{dy}-Ec\,Pr\left(\frac{du}{dy}\right)^2\right)\right)-\ldots$$

Comparing the coefficient of $p^0, p^1, p^2, p^3\ldots$, we obtain

$$p^0: \frac{d^2\theta_0}{dy^2}=0, \quad (11)$$

$$p^1: \frac{d^2\theta_1}{dy^2}=-Ec\,Pr\left(\frac{du}{dy}\right)^2, \quad (12)$$

$$p^2: \frac{d^2\theta_2}{dy^2}=-2Ec\,Pr\frac{du_0}{dy}.\frac{du_1}{dy}, \quad (13)$$

$$p^3: \frac{d^2\theta_3}{dy^2}=-2Ec\,Pr\frac{du_0}{dy}.\frac{du_2}{dy}-Ec\,Pr\left(\frac{du}{dy}\right)^2, \quad (14)$$

The boundary conditions are transformed as:

$$\theta_0(0)=1, \theta_1(0)=\theta_2(0)=\theta_3(0)=\ldots=0,$$
$$\theta_0(1)=\theta_1(1)=\theta_2(1)=\theta_3(1)=\ldots=0, \quad (15)$$

Similarly for equation (6) there is no initial approximation. Therefore, can be transformed as:

$$\frac{d^2u}{dy^2}=p\left[\frac{dP}{dx}-Gre\theta\right] \quad (16)$$

such that

$$u=u_0+pu_1+p^2u_2+p^3u_3+\ldots \quad (17)$$

Substituting equation (17) into equation (16), we obtain

$$\frac{d^2u_0}{dy^2}+p\frac{d^2u_1}{dy^2}+p^2\frac{d^2u_2}{dy^2}+\ldots=p\frac{dP}{dx}-pGre\theta_0-p^2Gre\theta_1-$$
$$p^3Gre\theta_3-\ldots \quad (18)$$

Comparing the coefficient of $p^0, p^1, p^2, p^3\ldots$, we obtain

$$p^0: \frac{d^2u_0}{dy^2}=0, \quad (19)$$

$p^1: \frac{d^2u_1}{dy^2} = \frac{dP}{dx} - Gre\theta_0,$ (20)

$p^2: \frac{d^2u_2}{dy^2} = -Gre\theta_1,$ (21)

$p^3: \frac{d^2u_3}{dy^2} = -Gre\theta_2,$ (22)

The boundary conditions for these equations are transformed as:

$u_0(0) = 1, u_1(0) = u_2(0) = u_3(0) = \ldots = 0,$

$u_0(1) = u_1(1) = u_2(1) = u_3(1) = \ldots = 0,$ (23)

Therefore solving equations (11) and (19) and applying the boundary conditions $\theta_0(0) = 1$and $\theta_0(1) = 0, u_0(0) = 0,$ and $u_0(1) = 0$, we obtain the solutions

$\theta_0 = A_1 y + A_2,$ (24)

$u_0 = B_1 y + B_2.$ (25)

Solving equations (12) and (20) and applying the boundary conditions $\theta_1(0) = 0$ and $\theta_1(1) = 0, u_1(0) = 0,$ and $u_1(1) = 0$, we obtain the solutions

$\theta_1 = -\frac{Ec\,Pr\,y^2}{2} + A_3 y + A_4,$ (26)

$u_1 = \frac{dP}{dx} y - Gre\left(\frac{y^2}{2} - \frac{y^3}{6}\right) + B_3 y + B_4.$ (27)

Solving equations (13) and (21) and applying the boundary conditions $\theta_2(0) = 0$ and $\theta_2(1) = 0, u_2(0) = 0,$ and $u_2(1) = 0$, we obtain the solutions

$\theta_2 = \frac{Ec\,Pr\,y^3}{3}\frac{dP}{dx} - Ec\,Pr\left(\frac{y^3}{3} - \frac{y^4}{12}\right) + Ec\,Pr\,B_3\,y^2 + A_5 y,$ (28)

$u_2 = \frac{Ec\,Pr\,Grey^4}{24} - \frac{GreA_3 y^3}{6} + B_5 y + B_6.$ (29)

Solving equations (14) and (22) and applying the boundary conditions $\theta_3(0) = 0$ and $\theta_3(1) = 0, u_3(0) = 0,$ and $u_3(1) = 0$, we obtain the solutions

$\theta_3 = \frac{Ec^2\,Pr^2\,Grey^5}{60} - \frac{Ec\,Pr\,GreA_3 y^4}{12} + Ec\,Pr\,B_5\,y^2 - \frac{Ec\,Pr\,y^4}{12}\left(\frac{dP}{dx}\right)^2 + Ec\,Pr\,G\,re\left(\frac{y^4}{12} - \frac{y^5}{20}\right) - Ec\,Pr\,G\,re^2\left(\frac{y^4}{12} - \frac{y^5}{20} + \frac{y^6}{120}\right) + Ec\,Pr\,G\,reB_3\left(\frac{y^3}{3} - \frac{y^4}{12}\right) - \frac{Ec\,Pr\,B_3^2 y^2}{2} - \frac{Ec\,Pr\,B_3 y^3}{3}\frac{dP}{dx} + A_7 y + A_8$ (30)

$u_3 = -\frac{Ec\,Pr\,Grey^5}{60}\frac{dP}{dx} + Ec\,Pr\,G\,re^2\left(\frac{y^5}{60} - \frac{y^6}{360}\right) - \frac{Ec\,Pr\,GreB_3 y^4}{12} - \frac{GreA_5 y^3}{6} + B_7 y + B_8.$ (31)

Where,

$A_1 = -1, A_2 = 1, B_1 = -1, B_2 = 1,$

$A_3 = \frac{EcPr}{2_{4_3}\frac{Gre}{3}\frac{1}{2}\frac{dP}{dx_4}}$

$A_5 = \frac{Ec\,Pr\,Gre}{4} - \frac{EcPr}{3\frac{dP}{dx}Pr\,B_{36}}$

$B_5 = \frac{GreA_3}{24} - \frac{Gre}{24}, B_6 = 0,$

$A_7 = \frac{Ec\,Pr\,GreA_3}{12} - \frac{Ec^2\,Pr^2\,Gre}{60} - Ec\,Pr\,B_5 + \frac{EcPr}{12}\left(\frac{dP}{dx}\right)^2 - \frac{Ec\,Pr\,Gre}{30} + \frac{Ec\,Pr\,B_3}{3}\frac{dP}{dx} + \frac{Ec\,Pr\,Gre^2}{24} - \frac{Ec\,Pr\,GreB_3}{4} + \frac{Ec\,Pr\,B_3^2}{2}, A_8 = 0,$

$B_7 = \frac{Ec\,Pr\,Gre}{60}\frac{dP}{dx} - \frac{Ec\,Pr\,Gre^2}{72} + \frac{Ec\,Pr\,GreB_3}{12} + \frac{GreA_5}{6}, B_8 = 0.$

To find the rate of heat transfer and skin friction between the fluid and the heated and cold plate are given by

$Nu_0 = -1 + A_3 + A_5 + A_7,$

$Nu_1 = -1 - Ec\,Pr + A_3 + Ec\,Pr\frac{dP}{dx} - \frac{7Ec\,Pr\,Gre}{12} + Ec\,Pr\,B_3 + A_5 + \frac{Ec^2\,Pr^2\,Gre}{12} - \frac{Ec\,Pr\,GreA_3}{3} + Ec\,Pr\,B_5 - \frac{EcPr}{3}\left(\frac{dP}{dx}\right)^2 - Ec\,Pr\,B_3\frac{dP}{dx} - \frac{2Ec\,Pr\,Gre^2}{15} + \frac{2Ec\,Pr\,GreB_3}{3} - Ec\,Pr\,B_3^2 + A_7.$

$\tau_0 = -1 + B_3 + B_5 + B_7,$

$\tau_1 = -1 + \frac{dP}{dx} - \frac{Gre}{2} + B_3 + \frac{Ec\,Pr\,Gre}{6} - \frac{GreA_3}{2} + B_5 - \frac{Ec\,Pr\,Gre}{12}\frac{dP}{dx} + \frac{Ec\,Pr\,Gre^2}{15} - \frac{Ec\,Pr\,GreB_3}{3} - \frac{GreA_5}{2} + B_7.$

To find the mass flux $Q = \int_0^1 u dy$, we have

$Q = \frac{1}{2} + \frac{dP}{6dx} - \frac{Gre}{8} + \frac{B_3}{2} + \frac{Ec\,Pr\,Gre}{120} - \frac{GreA_3}{24} + \frac{B_5}{2} - \frac{Ec\,Pr\,Gre}{360}\frac{dP}{dx} + \frac{Ec\,Pr\,Gre^2}{420} - \frac{E\,Pr\,GreB_3}{60} - \frac{GreA_5}{24} + \frac{B_7}{2}.$

To determine the pressure gradient in this problem, we assume that the flow has a constant mass flux. Using this assumption, we can calculate the pressure gradient that drives the flow.

$\int_0^1 u dy = q$ (32)

Where q is the constant mass flux. Then the pressure gradient can be expressed as:

$\frac{dP}{dx} = \frac{A_9 + A_{10}}{A_{11}}.$

Where,

$A_9 = -\frac{Ec\,Pr\,Gre^2}{420} + \frac{Ec\,Pr\,GreB_3}{60} + \frac{GreB_3}{24} - \frac{B_7}{2},$

$A_{10} = q - \frac{1}{2} + \frac{Gre}{8} - \frac{B_3}{2} - \frac{Ec\,Pr\,Gre}{120} + \frac{GreA_3}{24} - \frac{B_5}{2},$

$A_{11} = \frac{1}{6} - \frac{Ec\,Pr\,Gre}{360}$

To find the critical values of Gre after which a reverse flow sets in near the stationary plates, we evaluate $\frac{du}{dy}\Big|_{y=1} = 0$, and found that

$Gre_c = \frac{A_{12}}{A_{13}}$

Where,

$A_{12} = 1 - \frac{dP}{dx} + B_3 + B_5 + B_7,$

$A_{13} = \frac{EcPr}{6\frac{1A_3}{2\ 2} - \frac{EcPr}{12\frac{dP}{dx}\frac{EcPr}{3}}}$

RESULTS AND DISCUSSION

This research paper presents an analytical study of mixed convection flow in a vertical channel, considering the effects of viscous dissipation. The governing equations, along with the boundary conditions, are solved using the Homotopy Perturbation Method. Graphs are plotted to analyze the influence of key flow parameters. The rate of heat transfer, skin friction, and mass flux are numerically evaluated and discussed.

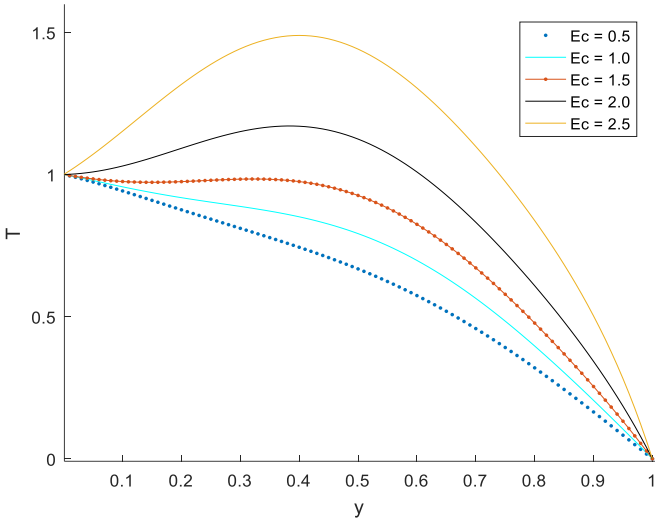

Figure 2: Temperature distribution for different values of Ec when $Pr = 0.71$ and $Gre = 30$

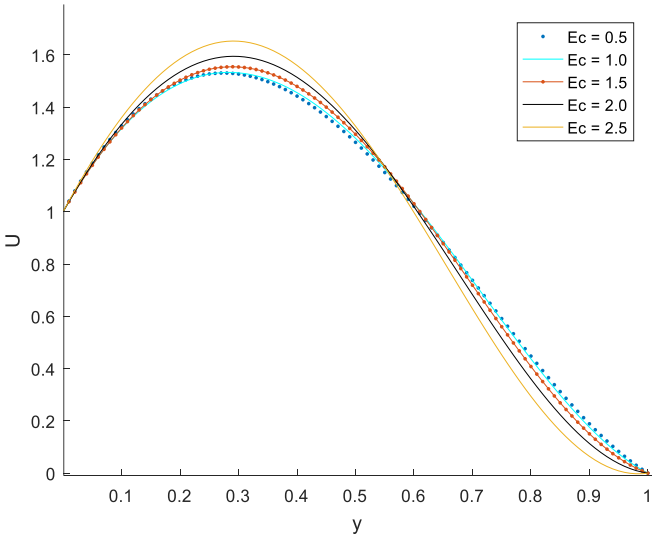

Figure 3: Velocity distribution for different values of Ec when $Pr = 0.71$ and $Gre = 30$

The effects of viscous dissipation on fluid temperature and velocity are illustrated in Figures 2 and 3. Notably, as viscous dissipation increases, the fluid velocity rises in the region near the heated plate, while it decreases in the region near the cold plate. However, the opposite pattern is observed for fluid temperature, as depicted in Figure 2.

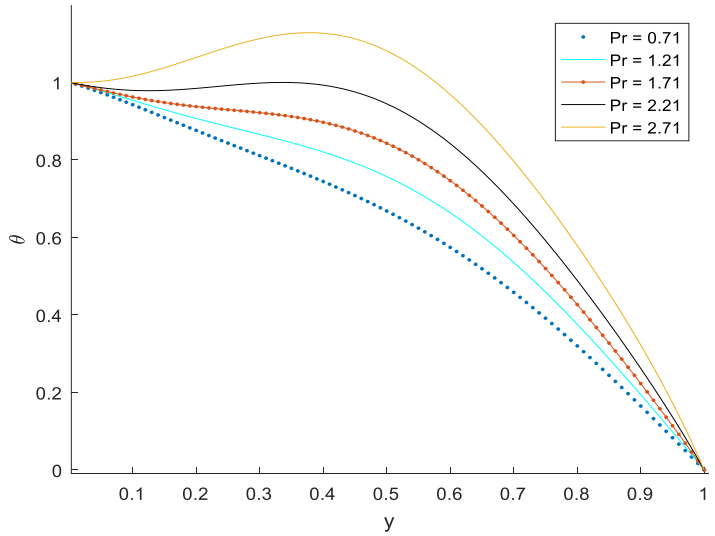

Figure 4: Temperature distribution for different values of Pr when $Ec = 0.5$ and $Gre = 30$

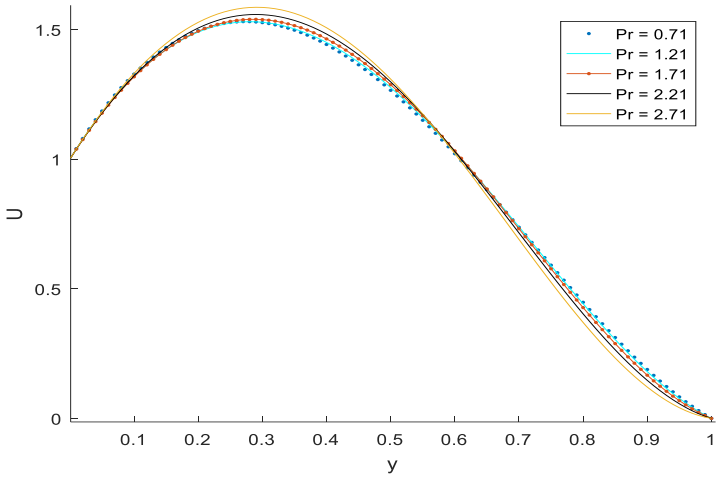

Figure 5: Velocity distribution for different values of Pr when $Ec = 0.5$ and $Gre = 30$

Figures 4 and 5 illustrate the behavior of temperature and velocity profiles with changes in the Prandtl number. From Figure 4, it is observed that the temperature profile increases as the Prandtl number rises. In contrast, Figure 5 shows that the velocity profile decreases near the heated plate with increasing Prandtl number, while it increases near the cold plate as the Prandtl number continues to grow.

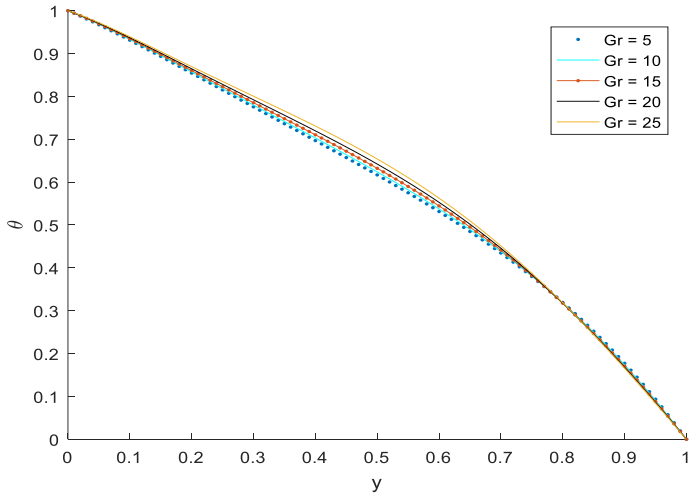

Figure 6: Temperature distribution for different values of Gre when $Ec = 0.5$ and $Pr = 0.71$

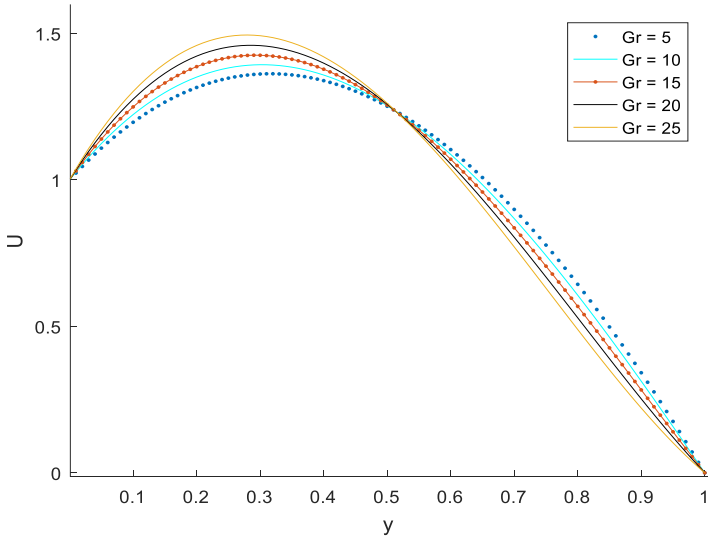

Figure 7: Velocity distribution for different values of Gre when $Ec = 0.5$ and $Pr = 0.71$

The effects of the mixed convection parameter on temperature and velocity profiles are shown in Figures 6 and 7. An increase in mixed convection produces two opposing trends in velocity within the channel. However, increasing the mixed convection parameter enhances the convection current within the channel.

Table 1: Critical values of Gre at the plate $y = 1$

	$Pr = 0.044, q = 1$	$Pr = 0.71, q = 1$	$Pr = 0.71, q = 2$
Ec	Gre_{c1}	Gre_{c1}	Gre_{c1}
0.2	79.90863	55.54312	35.02410
0.4	80.09052	55.61212	35.24108
0.6	80.41234	55.80512	35.50170
0.8	80.53140	55.98021	35.54212
1.0	80.60021	56.03210	35.56075

Table 1 highlights the critical values of the parameter(Gre) that indicate the onset of reverse flow near the stationary plate. It is observed that an increase in viscous dissipation raises the critical values of (Gre) associated with reverse flow near the plate. Conversely, both the reverse flow region and the critical values of the mixed convection parameter that cause flow reversal expand as the mixed convection parameter increases. Additionally, the table shows that the mixed convection parameter (Gre) decreases with higher Prandtl numbers.

Table 2: Estimated numerical values of rate of heat transfer at the plate $y = 0$ and $y = 1$

		$Gre = 10, q = 1$		$Gre = 15, q = 1$		$Gre = 15, q = 2$	
Ec	Pr	Nu_0	Nu_1	Nu_0	Nu_1	Nu_0	Nu_1
0.2		0.9877	1.0240	0.9855	1.0233	0.8889	1.1375
0.4		0.9755	1.0480	0.9712	1.0464	0.7783	1.2745
0.6	0.044	0.9634	1.0718	0.9571	1.0694	0.6683	1.4110
0.8		0.9515	1.0955	0.9432	1.0922	0.5588	1.5469
1.0		0.9396	1.1191	0.9294	1.1148	0.4499	1.6823
0.2		0.8146	1.3754	0.7886	1.3558	0.7270	3.1553
0.4		0.6559	1.7254	0.6221	1.6712	2.3161	5.1774
0.6	0.71	0.5225	2.0513	0.4969	1.9502	3.7711	7.0701
0.8		0.4132	2.3544	0.4091	2.1964	5.0958	8.8372
1.0		0.3266	2.6360	0.3548	2.4137	6.2940	10.4825

The numerical values for the rate of heat transfer on both plates are simulated and shown in Table 2. It is evident that as viscous dissipation increases, the rate of heat transfer decreases on the cold plates. Additionally, the heat transfer rate is higher when mercury is used as the working fluid compared to air.

Table 3: Estimated numerical values of skin friction at the plate $y = 0$ and $y = 1$

		$Gre = 10, q = 1$		$Gre = 15, q = 1$		$Gre = 15, q = 2$	
Ec	Pr	τ_0	τ_1	τ_0	τ_1	τ_0	τ_1
0.2		2.8308	3.1670	3.2459	2.7503	9.2415	8.7547
0.4		2.8282	3.1674	3.2419	2.7506	9.2331	8.7594
0.6	0.044	2.8257	3.1678	3.2378	2.7509	9.2246	8.7641
0.8		2.8232	3.1682	3.2338	2.7511	9.2162	8.7687
1.0		2.8207	3.1685	3.2298	2.7514	9.2078	8.7734
0.2		2.7930	3.1721	3.1860	2.7531	9.1150	8.8241
0.4		2.7541	3.1760	3.1259	2.7524	8.9839	8.8944
0.6	0.71	2.7168	3.1784	3.0696	2.7478	8.8566	8.9608
0.8		2.6810	3.1793	3.0173	2.7393	8.7333	9.0233
1.0		2.6467	3.1787	2.9687	2.7270	8.6137	9.0820

The numerical computations of skin friction on both plates are provided in Table 3. The table indicates that an increasing mixed convection parameter tends to raise the skin friction on both plates. Additionally, the skin friction decreases with increasing viscous dissipation on the cold plate, while it increases with higher viscous dissipation on the heated plate.

Table 4: Estimated numerical values of pressure gradient

		$Gre = 10, q = 1$	$Gre = 15, q = 1$	$Gre = 15, q = 2$
Ec	Pr	$\frac{dP}{dx}$	$\frac{dP}{dx}$	$\frac{dP}{dx}$
0.2		−0.9881	1.5203	−10.4797
0.4		−0.9761	1.5404	−10.4595
0.6	0.044	−0.9642	1.5608	−10.4392
0.8		−0.9515	1.5811	−10.4189
1.0		−0.9396	1.6014	−10.3986
0.2		−0.8073	1.8271	−10.1729

0.4		−0.6146	2.1542	−9.8458
0.6	0.71	−0.4219	2.4813	−9.5187
0.8		−0.2291	2.8084	−9.1916
1.0		−0.0364	3.1355	−8.8645

Table 4 presents the numerical values of the pressure gradient. It is observed that the pressure gradient decreases with increasing viscous dissipation. However, the pressure gradient increases as the mixed convection parameter rises.

Table 5: Estimated numerical values of mass flux Q

		$Gre = 10, q = 1$	$Gre = 15, q = 1$
Ec	Pr	Q	Q
0.2		0.87513	0.88946
0.4		0.85126	0.86300
0.6	0.044	0.81273	0.79605
0.8		0.78473	0.79001
1.0		0.74100	0.75103
0.2		1.26314	1.52160
0.4		1.05141	1.26601
0.6	0.71	1.02011	1.20070
0.8		1.00619	1.18107
1.0		0.91250	1.13440

Table 5 displays the numerical values of mass flux. It is observed that mass flux increases with rising viscous dissipation. Additionally, mass flux is higher when air is used as the working fluid compared to mercury. In other words, an increasing Prandtl number tends to enhance mass flux.

Table 6: Numerical of numerical values of present problem and that of Tafida and Muawiya (2019)

	Tafida and Muawiya (2019) $Gre = 10, y = 0.5$		Present Problem $Gre = 10, Pr = 0.71, \frac{dP}{dx} = 0, y = 0.5$	
Ec	Temperature	Velocity	Temperature	Velocity
0.2	0.46083	0.53986	0.46197	0.53954
0.4	0.44172	0.53129	0.44180	0.53127
0.6	0.42086	0.52976	0.42088	0.52959
0.8	0.40026	0.50180	0.40030	0.50183
1.0	0.39679	0.49079	0.39682	0.49090

To validate this study, we compared our results for temperature and velocity with those of Tafida and Muawiya (2019) and found strong agreement between them. This indicates that the Homotopy Perturbation Method is an effective tool for solving coupled and nonlinear differential equations. Furthermore, we have enhanced Tafida and Muawiya's (2019) work by incorporating the mixed convection parameter. The comparison is shown in Table 6.

CONCLUSION

This article presents an analytical study of mixed convection flow in a vertical channel, considering the effects of viscous dissipation. The following conclusions can be drawn from the investigation:

i. Fluid velocity increases in the region near the heated plate, while it decreases in the area adjacent to the cold plate as viscous dissipation increases.
ii. The pressure gradient rises with an increase in the mixed convection parameter.
iii. The mass flux is greater when air is used as the working fluid compared to mercury.
iv. The mixed convection parameter (Gre) decreases due to a higher Prandtl number.

REFERENCES

Abdulhakeem, Y., Abdulrahman, B. and Nasiru, O. S. (2022). Boundary layer analysis flow past a porous rotating disk with Dufour and soret effects. *FUDMA Journal of Sciences (FJS). 6(2): 49 – 57*

Ajibade, A. O. and Princely, O. O. (2020). Effect of viscous dissipation on steady natural convection, heat and mass transfer in a vertical channel with variable viscosity and thermal conductivity. *Journal of Heat and Mass Transfer Research. 7: 105 – 116*

Ajibade, A. O. and Tafida, M. K. (2020). Effects of variability in viscosity and thermal conductivity Couette flow and heat transfer. *Transactions of NAMP vol.11, (January – June, 2020 Issue).*

Ajibade, A. O. and Tafida, M. K. (2022). Viscous dissipation effect of on steady natural Convection Couette flow with convective boundary condition. *International Journal of Non-Linear Sciences and Numerical Simulation (IJNSNS). 7: 105 – 116*

Ajibade, A. O., Ayuba, M. U. and Tafida, M. K. (2021). An Analytical study on effects of viscous dissipation and suction/injection on a steady MHD natural convection Couette flow of heat generating/absorbing fluid. *Advances in Mechanical Engineering. 13(5), 1 – 12.*

Biazar, J. and Ghazvini (2008). Homotopy perturbation method for solving hyperbolic partial differential equations. *International Journal of Computers and Mathematics with Applications. 56: 453 – 458.*

Essam, M. E. and Mohammed, S. A. (2021). Mixed convection hybrid-nanofluid in a vertical channel under the effect of thermal radiative flux. *Case Studies in Thermal Engineering. 25, 100913.*

Fahad, B. M., Samad, M. A and Hossain, M. R. (2017). Combined effect of viscous dissipation and radiation on an unsteady natural convection. *Am. J. Comput. Appl. Math. 7(3): 71 – 79*

Gebhart B. (1962). Effect of viscous dissipation on natural convection. *Journal of Fluid Mechanics. 14: 225 – 232*

Hamida, N., Mulyano, Nurul, M. S. and Salisa, BR. S (2023). Exploring of Homotopy Perturbation Method for solving spread of Covid-19. *Jambura Journal of Biomathematics. 4(2), 138 – 145.*

Henniche, R. and Abdelkader, K. (2020). Mixed convection in a vertical channel by addition of staggered inclined baffles. *Journal of Thermophysics and Heat Transfer. Doi:10.2514/1.T6037.*

Kairi, R. R., Murthy, P. N and Ng, C. (2011). Effect of viscous dissipation in a Non-Darcy porous medium saturated with Non-Newtonian fluid of variable viscosity. *The Open Transport Phenomena Journal. 3: 1 – 8*

Muawiya, H. U. and Tafida, M. K. (2019). Viscous dissipation effects on steady natural convection Couette flow in a vertical channel. *Wudil Journal of Pure and Applied Sciences. 1(2), 169 – 179.*

Muneer, A. I., Ahmed, K. H., Faton, M. O. and Lioua, K. (2020). Effect of Driven Sidewalls on Mixed Convection in an Open trapezoidal cavity with a channel. *Journal of Heat Transfer. 142/082601 – 1.*

Nur, S. W., Noriham, Md. A., Najiyah, S. K., Ioan, P., Norfifah, B. and Mohd, E. H. (2022). Magnetohydrodynamics mixed convection flow of a hybrid nanofluid past a permeable vertical flat plate with thermal radiation effect. *Alexandria Engineering Journal. 6, 3323 – 3333.*

Sheid, A. M., Oyom, O. A., Momoh, D. S., and Onojovwo, T. F. (2023). Convective heat and Casson nanofluid flow over a vertical plate with heat source. *FUDMA Journal of Sciences (FJS). 7(2): 9 – 18*

Tafida, M. K. and Ajibade, A. O. (2020). Variable viscosity and viscous dissipation effects on free convective Couette flow in a vertical channel: The Homotopy perturbation method approach. *The Journal of the Mathematical Association of Nigerian. 47(1), 161 – 175.*

Yusuf, A. B. and Ajibade, A. O. (2020). Combined effects of variable viscosity, viscous dissipation and thermal radiation on unsteady natural convection Couette flow through a vertical porous channel. *FUDMA Journal of Sciences (FJS). 4(2): 135 – 150*

Yusuf, A. B. and Ajibade, A. O. (2018). Unsteady natural convection flow through a vertical porous channel filled with porous material under the effect of thermal radiation. *FUDMA Journal of Sciences (FJS). 2(2): 101 – 115*